SCIENTIFIC REPORTS

OPEN

Simultaneous observation of free and defect-bound excitons in $CH_3NH_3PbI_3$ using four-wave mixing spectroscopy

Received: 12 September 2016
Accepted: 17 November 2016
Published: 15 December 2016

Samuel A. March, Charlotte Clegg, Drew B. Riley, Daniel Webber, Ian G. Hill & Kimberley C. Hall

Solar cells incorporating organic-inorganic perovskite, which may be fabricated using low-cost solution-based processing, have witnessed a dramatic rise in efficiencies yet their fundamental photophysical properties are not well understood. The exciton binding energy, central to the charge collection process, has been the subject of considerable controversy due to subtleties in extracting it from conventional linear spectroscopy techniques due to strong broadening tied to disorder. Here we report the simultaneous observation of free and defect-bound excitons in $CH_3NH_3PbI_3$ films using four-wave mixing (FWM) spectroscopy. Due to the high sensitivity of FWM to excitons, tied to their longer coherence decay times than unbound electron- hole pairs, we show that the exciton resonance energies can be directly observed from the nonlinear optical spectra. Our results indicate low-temperature binding energies of 13 meV (29 meV) for the free (defect-bound) exciton, with the 16 meV localization energy for excitons attributed to binding to point defects. Our findings shed light on the wide range of binding energies (2–55 meV) reported in recent years.

The efficiency of solar cells using organometal halide perovskite semiconductor absorber layers has skyrocketed during the past few years, now reaching a level competitive with existing solar cell technologies[1] while offering a low-cost solution-processed device platform. This has stimulated intense research into the fundamental photophysical properties of these materials[2–24]. A parameter that has received considerable attention recently is the exciton binding energy (E_b), which determines the primary mechanism of carrier transport during device operation. Unlike inorganic solar cell materials such as III-V semiconductors, in which sharp exciton resonances greatly simplify extraction of E_b, the solution-processed organometal halide perovskites possess substantial broadening due to defects[25] and intrinsic dynamic disorder associated with the freedom of orientation of methylammonium ions[26,27]. The broadening associated with these effects, which has been found to vary from 30 meV at cryogenic temperatures to 60 meV at room temperature[15], is comparable to (or larger than) the exciton binding energy. This broadening complicates the extraction of E_b from absorption or ellipsometry techniques[16]. In addition, while photoluminescence provides an effective probe of defect-induced localization and recombination processes[5,6], these techniques cannot isolate transitions relevant to absorption within an operational solar cell and can be hampered by incomplete phase transitions[6,15]. Extraction of E_b from magneto absorption techniques is also complicated by the strong broadening in the organometal halide perovskites, resulting in the need to use large magnetic fields (~20 Tesla)[9,10]. Due to these challenges, even for the most widely studied material $CH_3NH_3PbI_3$, the value of E_b has been quite controversial, with reports ranging from 2 meV to 55 meV[2–4,7–19].

Here we apply femtosecond four-wave mixing spectroscopy (FWM) to probe excitonic resonances in $CH_3NH_3PbI_3$. In this technique, two coherent ultrafast laser pulses described by electric fields $\vec{E}_1$ and $\vec{E}_2$ with wave vectors $\vec{k}_1$ and $\vec{k}_2$ excite a polarization component that emits light with wavevector $2\vec{k}_2 - \vec{k}_1$ (see Fig. 1). Measurement of the emitted light versus the detection photon energy and the time delay between the two incident laser pulses provides a wealth of information about the optical transitions within the system under study, including the resonance frequencies and the time scale for scattering processes that cause decay of coherence (the so-called dephasing time, T_2)[28]. For semiconductors, FWM is highly sensitive to excitons because the signal at

Department of Physics and Atmospheric Science, Dalhousie University, Halifax, Nova Scotia B3H 4R2 Canada. Correspondence and requests for materials should be addressed to K.C.H. (email: Kimberley.Hall@dal.ca)

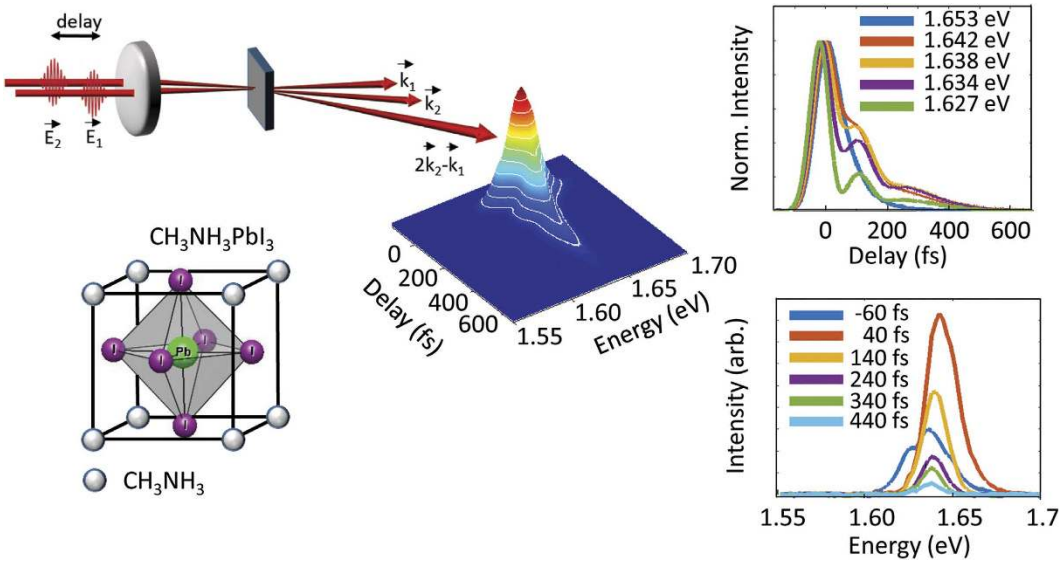

Figure 1. Upper left, schematic of four-wave mixing spectroscopy. Two 40 fs input pulses $\vec{E}_1$ and $\vec{E}_2$ excite a carrier density grating, and the self-diffracted signal along $2\vec{k}_2 - \vec{k}_1$ is measured using a monochromator and photomultiplier detector as a function of the time delay. **Lower left**, methylammonium lead iodide perovskite ABX_3, with $A = CH_3NH_3$, B = Pb, X = I. **Center** FWM response of the $CH_3NH_3PbI_3$ sample at 10 K for excitation at 1.653 eV, 11 meV above the band gap. **Upper Right**, FWM signal at fixed values of detection photon energy, showing a smooth decay (oscillations) for energies above (below) band gap. **Lower right**, FWM spectrum at fixed values of time delay, indicating multiple spectrally-distinct signal contributions.

each pulse delay is measured using a slow detector, so that the magnitude of the signal is dictated by the coherence lifetime of the transition. Excitons, being charge-neutral spatially-localized excitations, have much longer T_2 times than delocalized free carrier and band tail transitions[29,30]. This sensitivity to excitonic effects has been exploited to observe the fundamental exciton in LT-GaAs[31], in which the optical band edge is strongly broadened by As_{Ga} antisite defects preventing the observation of any signature of the exciton in linear absorption, as well as the exciton resonance at the spin-orbit split-off band gap in InP[32], which is masked in linear spectroscopy by strong degenerate interband transitions associated with the lower-energy band gaps.

Our experiments reveal two discrete resonances below the band gap of the $CH_3NH_3PbI_3$ thin films, which we attribute to the free exciton transition and a defect-bound exciton transition. The simultaneous observation of both free and localized excitons using this absorption-based nonlinear optical technique shows that both types of exciton can contribute to absorption during operation of a solar cell. At 10 K, the excitonic resonances we observe occur at 1.629 eV and 1.613 eV. The 16 meV energy separation is attributed to the binding energy of excitons to point defects within the perovskite film[25], and is in reasonable agreement with the recent measurement of an exciton localization energy of 17 meV in $CH_3NH_3PbI_{3-x}Cl_x$ using photoluminescence and THz techniques[5]. Our measured transition energies correspond to an exciton binding energy of 13 meV (29 meV) for the free (defect-bound) exciton at 10 K, with a negligible temperature dependence up to 40 K. The low-temperature free exciton binding energy we measure is in reasonable agreement with the value of 16 meV determined at 2 K from recent magneto-optical studies at high magnetic fields[9,10]. Together with the difficulty in fully characterizing the dielectric constant including the potential contributions of phonons[13,17] and related dispersion[19], the close proximity of the free and bound exciton states we observe has likely contributed to the broad range of exciton binding energies reported in the literature[2–4,7–19,22].

Results and Discussion

The four-wave mixing signal measured on the $CH_3NH_3PbI_3$ sample at 10 K is shown in Fig. 1. For these results, the center photon energy of the laser spectrum was 1.653 eV, 11 meV above the band gap determined from linear absorption measurements (Fig. S1). The FWM spectrum exhibits a strong dependence on the time delay between the exciting laser pulses, as shown in the lower right panel of Fig. 1. For time delays on the rising edge of the FWM signal, the spectrum consists of three peaks. The lowest energy peak has a maximum between 1.62 eV and 1.63 eV, with a tail on the low energy side. The other two peaks occur at approximately 1.635 eV and 1.648 eV. The FWM signal reaches its maximum intensity around zero delay, characterized by a broad response encompassing a range of energies above and below the band gap. For longer delays, the signal narrows spectrally and decays on a time scale of a few hundred femtoseconds. Cuts through the two-dimensional FWM results versus time delay are displayed in the upper right panel of Fig. 1. The signal exhibits a smooth temporal decay for detection energies above the band gap, while for energies below the band gap oscillations appear. These oscillations resemble beating effects observed in FWM studies in the presence of simultaneous responses due to bound and free excitons in GaAs superlattices[33] and exciton and trion resonances in doped CdTe quantum wells[34]. Together with the observation

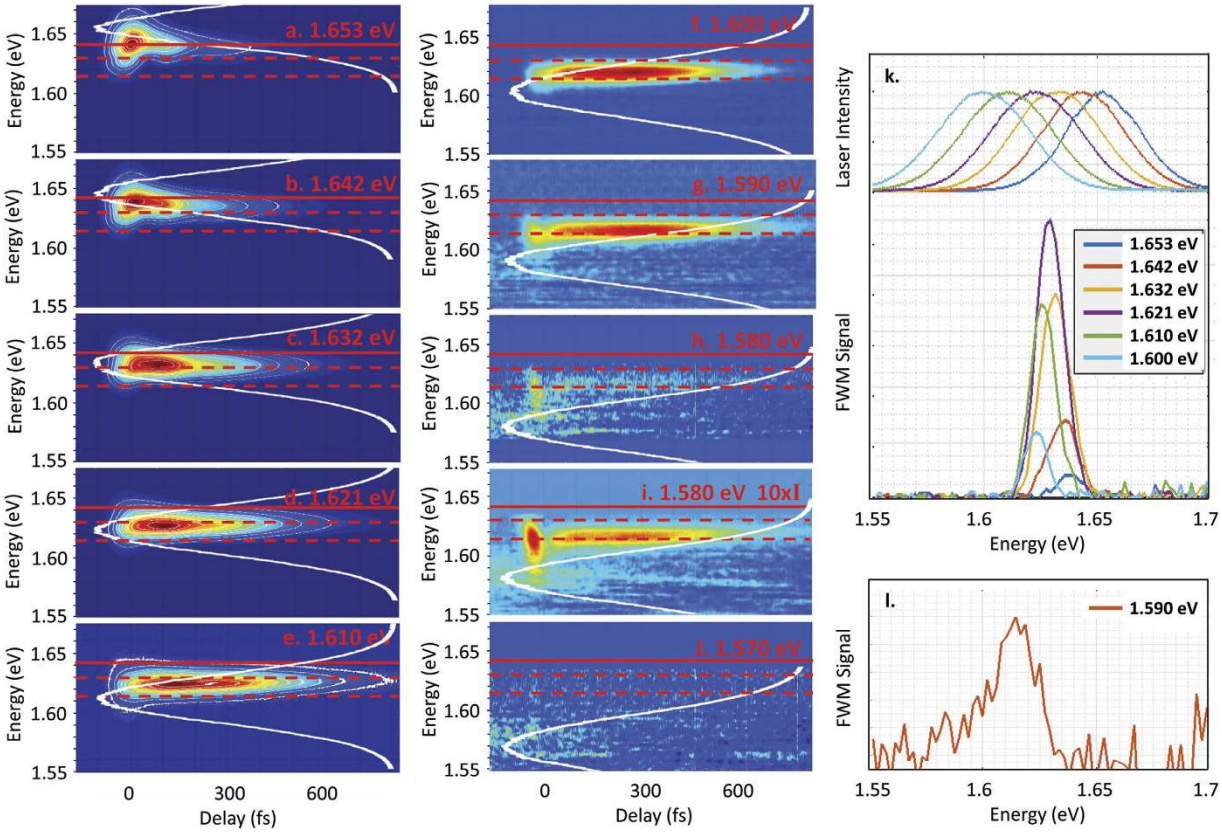

Figure 2. (**a**–**j**) FWM response of $CH_3NH_3PbI_3$ for varying laser tuning relative to the band gap. The FWM signal is displayed using a colored contour scale. The white curve overlaid on the FWM results indicates the laser spectrum. The solid red line indicates the 10 K band gap determined from linear absorption. The two dashed lines indicate the resonance energies of 1.613 eV and 1.629 eV determined for the defect-bound and free exciton transition, respectively. The defect-bound exciton appears as a weak, spectrally-isolated peak when the laser is tuned well below band gap (**g**–**i**). The free exciton resonance, which produces a much stronger FWM signal than the bound exciton, is evident from the dependence of the FWM signal amplitude on laser tuning (**k**). In (**k**) the laser spectra are vertically offset from the FWM spectra. The free exciton dominates the four-wave mixing signal for time delays longer than 200 fs: results for 540 fs delay are shown in (**k**). (**l**) FWM spectrum at zero delay for excitation at 1.590 eV, showing the defect-bound exciton peak. The intensity of the 1.590 eV excitation laser pulses was 10 times larger for the results in **i**, permitting the defect-bound exciton to be observed more clearly.

of three peaks in the four-wave mixing spectrum, this suggests that there are multiple, distinct contributions to the measured FWM response of the perovskite film.

Further insight into the transitions contributing to the FWM response may be gained by performing measurements for which the laser pulses used to excite the sample are tuned relative to the band gap energy. The results of these experiments are shown in Fig. 2. In each panel, the laser spectrum is indicated by the white curve overlaid on the FWM signal, and the solid red line shows the band gap energy. For all experiments, the laser pulse fluence summed over the two excitation beams was held constant at 4 μJ/cm^2. The existence of a separate contribution to the FWM signal below the band gap is already apparent at early delays from the shape of the contours in the results for excitation at 1.653 eV in Fig. 2a. The broadband signal at higher energies in Fig. 2a is attributed to free carrier transitions[35] and transitions within the Urbach band tail[24,20,30]. As the laser is tuned below the band gap energy (Fig. 2b–i), the peak below the band gap grows in intensity relative to the free carrier response. When the laser is tuned to 1.580 eV, only the tail of the laser spectrum weakly excites the low-energy resonance, isolating it from other contributions, indicating a center energy of 1.613 eV and a spectral width of ~18 meV (Fig. 2l). When the laser pulses are tuned to 1.570 eV or lower energies, the laser spectrum has negligible overlap with the 1.613 eV peak, and no FWM signal is detected. The discrete resonance we observe in the FWM signal at 1.613 eV is attributed to an excitonic transition within the $CH_3NH_3PbI_3$ film.

The variation of the magnitude of the FWM signal as the laser pulses are tuned indicates that the resonance feature at 1.613 eV is not the only discrete resonance below the band gap. A stronger resonance occurs at higher energies, as shown in Fig. 2k, where the FWM spectrum at 540 fs delay is displayed color-coded with the corresponding laser spectrum in the upper panel. This second resonance has a maximum at 1.629 eV, with a width of 15 meV. The variation of the spectral content of the FWM signal as the laser is tuned indicates inhomogeneous broadening. Both of the resonances at 1.613 eV and 1.629 eV have spectral widths smaller than the laser pulse

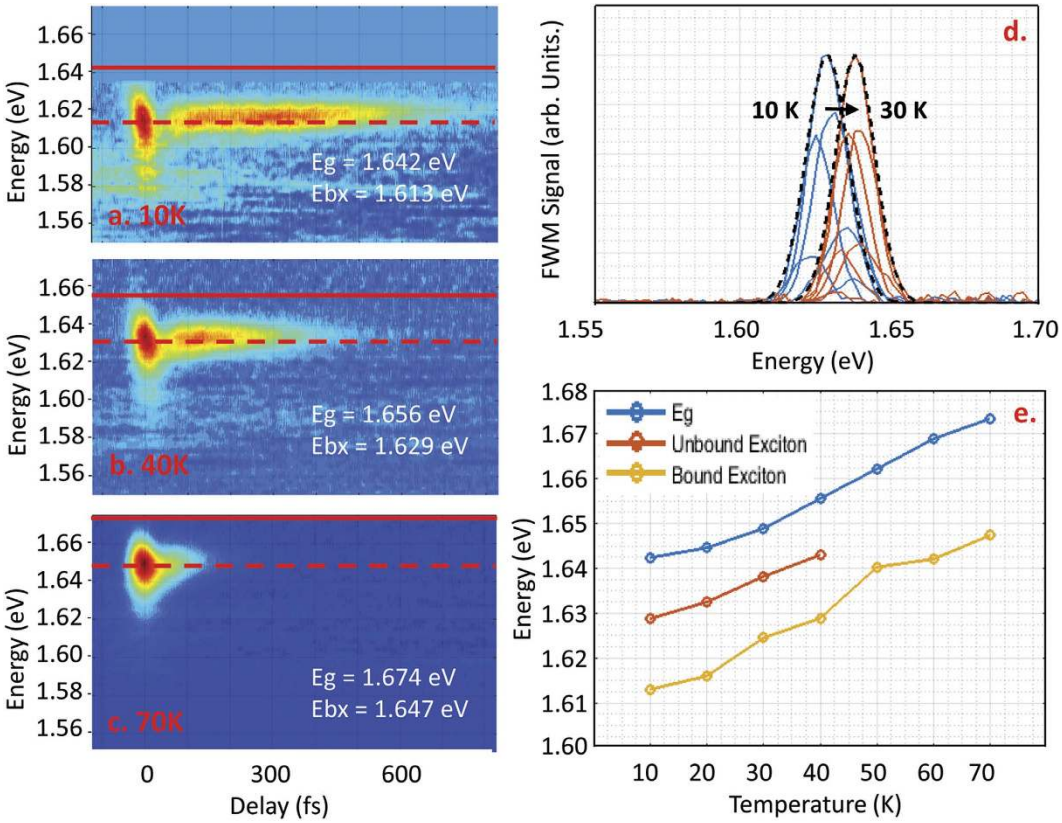

Figure 3. FWM response of the defect-bound exciton at (**a**) 10 K, (**b**) 40 K and (**c**) 70 K. with the corresponding bandgap indicated by the solid line. (**d**) FWM spectrum at 540 fs delay for a variety of spectral tunings, showing the variation in the resonance energy of the free exciton as the temperature is increased from 10 K (blue curves) to 30 K (red curves). The black dashed curves indicate a Gaussian fit to the resonance at each temperature. (**e**) The exciton transition energies deduced from the FWM results as a function of temperature. Both exciton resonance energies follow the temperature dependence of the band gap within the experimental uncertainty, indicating no discernible temperature dependence of the exciton binding energies within the accessible range.

bandwidth and have transition energies that are fixed as the center photon energy of the laser spectrum is varied. These features are reflective of discrete, excitonic transitions within the semiconductor. The strong 1.629 eV resonance is attributed to the free exciton transition, while the weaker resonance at 1.613 eV is attributed to an exciton bound to defects within the perovskite film. From a comparison of the transition energy of each exciton with the band gap energy, we determine the binding energies of these excitons to be 13 meV and 29 meV, respectively. The temperature-dependence of the FWM response from the two excitons is shown in Fig. 3. The free exciton resonance energy could only be determined up to 40 K due to the limited tuning range of the laser relative to the band gap at higher temperatures. The spectral position of the free and defect-bound exciton resonances both track the temperature dependence of the band gap energy, indicating no discernible dependence of the binding energies of the excitons on temperature below 40 K.

The binding energy of 13 meV we measured for the free exciton is in line with the value of 16 meV found from recent magneto-optical measurements at 2 K[9,10]. In refs 9 and 10, large magnetic fields (~20 Tesla) enabled the observation of the 2 s exciton transition, constraining the value of the binding energy over a much narrower range than in earlier magneto-optical experiments[7,8]. In our FWM experiments, the free exciton was found to contribute much more strongly than the bound exciton. Together with the higher sensitivity of FWM to excitonic resonances than linear absorption experiments, this accounts for the fact that the bound exciton was not observed in refs 9,10. The binding energy of the free and defect-bound exciton resonances we observe are both within the large spread of reported values of 2–55 meV for $CH_3NH_3PbI_3$[2–4,7–19], shedding some light on the controversy surrounding E_b in recent years. The uncertainty in determining the dielectric constant, including both the choice of appropriate spectral range[22] and the complexity tied to the role of lattice vibrations[13,17,19], has also contributed substantially to the wide range of reported binding energies since this value is essential to the modeling of absorption and photoluminescence. Since the transition energies of the free and defect-bound excitons are determined directly using FWM spectroscopy, no modeling is needed and the dielectric constant is not required to determine the binding energies. We note that in a recent work by Even *et al.*, the dielectric constant was taken as a fitting variable in modeling the linear absorption spectrum, yielding a free exciton binding energy of 13 meV at 80 K, in agreement with the value reported here.

The separation between the free and defect-bound exciton resonances is 16 meV. We attribute this to the binding energy of excitons to point defects within the $CH_3NH_3PbI_3$ film. The energy levels tied to a variety of

point defects were calculated using density functional theory techniques by Yin *et al.*[25]. All point defects with low formation energies were found to be shallow defects, with energies less than 50 meV away from the band extrema. The reported transition energies in ref. 25 suggest that the dominant donor MA_i may be responsible for exciton localization at low temperatures in our sample. The small 16 meV binding energy of these defects is consistent with a similar coherence decay time observed for the free and defect-bound excitons in our experiments (Fig. S2), which is a signature of weak localization[36]. Our findings are also in line with an exciton localization energy of 17 meV determined from photoluminescence and THz studies on $CH_3NH_3PbI_{3-x}Cl_x$[5]. Static disorder associated with the frozen methylammonium cations at low temperatures[13,27] may contribute to inhomogeneous broadening of the exciton resonances, which is reflected by the measured linewidths being ~5 times larger than the homogeneous width estimated from the duration of the coherent emission. As the localization energy is determined here with a precision of a few meV (limited by the level of inhomogeneous broadening), the 16 meV value we report will support theoretical models of point defects in $CH_3NH_3PbI_3$.

Multiple emission peaks have also been observed in photoluminescence experiments on single crystals of $CH_3NH_3PbI_3$[21], however the energy separation between the emitting exciton resonances was considerably larger than that found using FWM techniques in this work. As FWM detects the states participating in absorption, this suggests that carriers relax into deeper energy levels prior to radiative recombination. Our observations, which verify the existence of weakly localized exciton states in this system, are in agreement with recent power-dependent photoluminescence studies which determined that excitons recombine radiatively from trap states[5] and transient photoconductivity experiments that indicated a resonant transition below the band gap tied to localized states[23]. Our findings are also consistent with earlier four-wave mixing experiments in disordered III-V superlattices revealing simultaneous signatures of free excitons and excitons bound to neutral Carbon acceptors[33].

Conclusions

The application of coherent nonlinear optical spectroscopy to $CH_3NH_3PbI_3$ reported here complements and extends the numerous studies of this system using linear optical techniques in recent years, for which the substantial broadening inherent to the disordered organic inorganic perovskite materials obscures fundamental photophysical properties such as excitonic effects, leading to challenges in assessing crucial parameters for solar cell design. Since FWM preferentially detects optical species possessing long coherence decay times, this technique is highly sensitive to excitonic transitions, a feature that has been exploited for studying excitons in clean and disordered III-V and II-VI semiconductors over more than two decades[29,31–34]. The direct observation of the resonance energies of both free and defect-bound excitons in $CH_3NH_3PbI_3$, eliminating the need to rely on assumed values of the dielectric constant for determination of the associated binding energies, aids in clarifying the broad range of values of the exciton binding energy reported in recent years as the relative role of free and defect-bound excitons will vary depending on whether absorption or photoluminescence based detection schemes are utilized. The observation of defect-bound excitons using a technique based on nonlinear absorption indicates that both free and localized exciton species play a role in an operational solar cell. The measured localization energy for bound excitons of 16 meV reported here provides input to theoretical models of defects in $CH_3NH_3PbI_3$. Our findings demonstrate the power of FWM spectroscopy for studying excitonic properties and the influence of disorder in $CH_3NH_3PbI_3$, laying the foundation for studies on other materials within the organometal halide perovskite class of semiconductors, and will aid in improving solar cell device performance using these materials.

Methods

$CH_3NH_3PbI_3$ thin-film preparation. A modified sequential deposition procedure was used to prepare the thin film $CH_3NH_3PbI_3$ perovskite sample[37]. A 1 M PbI_2 solution in Diethylformamide (DMF), which was maintained at 70 °C throughout the deposition, was first stirred for 10 hours and then passed through a 0.45 μm pore PTFE filter into a clean glass vial heated to 70 °C. 300 μL of the solution was cast onto a room temperature, stationary sapphire substrate, which was subsequently spun at 5000 rpm for 60 seconds. Residual solvent was removed by immediately transferring the substrate to a 70 °C hotplate for 15 minutes. 300 μL of methylammonium iodide solution in isopropanol was deposited onto the spinning lead-iodide film (4000 rpm, 60 seconds). The films were annealed at 100 °C for 2 hours under an argon atmosphere. X-ray diffraction studies were carried out on a companion sample grown with the same recipe, and indicated no residual lead iodide. Prior to optical measurements, the completed samples were transferred into a portable liquid helium flow-through optical cryostat within an argon glovebox and sealed prior to removal of the cryostat to air. The cryostat was then evacuated for low-temperature optical studies under vacuum. The band gap was extracted from linear absorption measured by a CARY UV-VIS spectrometer following the findings of Even[13], which place it close to the peak of the absorption at low temperatures due to the combined influence of Sommerfeld enhancement and the free exciton transition. Scanning electron microscopy measurements on the sample indicate uniform polycrystalline morphology (see Supplementary Information for further details).

Two-pulse degenerate four-wave mixing. Ultrashort pulses are generated by a Ti:Sapphire mode-locked laser source, pumped by a solid state Nd:Vanadate laser, and passed through a group-velocity dispersion compensator prior to entering the four-wave mixing setup. A beam splitter produces two pulses with electric fields $\vec{E}_1$ and $\vec{E}_2$ that are focused in a noncollinear geometry onto the sample (with wave vectors $\vec{k}_1$ and $\vec{k}_2$). These pulses excite a spatially modulated carrier density that leads to a coherent polarization emitted with wave vector $2\vec{k}_2 - \vec{k}_1$, often referred to as a self-diffraction process. For a simple two-level system without interactions, the decay of the four-wave mixing signal as a function of the interpulse delay yields the decay time of quantum coherence on the optical transition. The FWM setup incorporates noise reduction via the rapid scan method using a

speaker-mounted retroreflector. A zero background autocorrelation, detected through the second harmonic generation of the two input pulses at an equivalent focus to the sample position, is used to optimize and measure the pulse duration and to maximize beam spatial overlap. The pulse duration at the sample position with optimized group-velocity dispersion compensation is approximately 40–50 fs, depending on the center photon energy of the laser spectrum. The four-wave mixing signal is sent through a monochromator, and is detected using a photomultiplier tube (PMT). For more details on the four-wave mixing technique, see ref. 38.

References

1. Best Research-Cell Efficiencies. http://www.nrel.gov/pv/assets/images/efficiency_chart.jpg (2016). Online; accessed 9 November 2016.
2. Wu, K. *et al.* Temperature-dependent excitonic photoluminescence of hybrid organometal halide perovskite films. *Phys. Chem. Chem. Phys.* **16,** 22476–22481, doi: 10.1039/C4CP03573A (2014).
3. Savenije, T. J. *et al.* Thermally activated exciton dissociation and recombination control the carrier dynamics in organometal halide perovskite. *Journal of Physical Chemistry Letters* **5,** 2189–2194, doi: 10.1021/jz500858a (2014).
4. Sun, S. *et al.* The origin of high efficiency in low-temperature solution-processable bilayer organometal halide hybrid solar cells. *Energy Environ. Sci.* **7,** 399–407, doi: 10.1039/c3ee43161d (2014).
5. He, H. *et al.* Exciton localization in solution-processed organolead trihalide perovskites. *Nat. Commun.* **7,** 10896, doi: 10.1038/ncomms10896 (2016).
6. Wehrenfennig, C., Liu, M., Snaith, H. J., Johnston, M. B. & Herz, L. M. Charge carrier recombination channels in the low-temperature phase of organic-inorganic lead halide perovskite thin films. *APL Mater.* **2,** 081513, doi: 10.1063/1.4891595 (2014).
7. Tanaka, K. *et al.* Comparative study on the excitons in lead-halide-based perovskite-type crystals $CH_3NH_3PbBr_3CH_3NH_3PbI_3$. *Solid State Communications* 619–623, doi: 10.1016/S0038-1098(03)00566-0 (2003).
8. Hirasawa, M., Ishihara, T., Goto, T., Uchida, K. & Miura, N. Magnetoabsorption of the lowest exciton in perovskite-type compound $(CH_3NH_3)PbI_3$. *Physica B: Physics of Condensed Matter* **201,** 427–430, doi: 10.1016/0921-4526(94)91130-4 (1994).
9. Miyata, A. *et al.* Direct measurement of the exciton binding energy and effective masses for charge carriers in organic-inorganic tri-halide perovskites. *Nature Physics* **11,** 582–587, doi: 10.1038/nphys3357 (2015).
10. Galkowski, K. *et al.* Determination of the exciton binding energy and effective masses for methylammonium and formamidinium lead tri-halide perovskite semiconductors. *Energy Environ. Sci.* **9,** 962–970, doi: 10.1039/C5EE03435C (2016).
11. Lin, Q., Armin, A., Nagiri, R. C. R., Burn, P. L. & Meredith, P. Electro-optics of perovskite solar cells. *Nature Photonics* **9,** 106–112, doi: 10.1038/nphoton.2014.284 (2015).
12. Saba, M. *et al.* Correlated electron-hole plasma in organometal perovskites. *Nature communications* **5,** 5049, doi: 10.1038/ncomms6049 (2014).
13. Even, J., Pedesseau, L. & Katan, C. Analysis of multivalley and multibandgap absorption and enhancement of free carriers related to exciton screening in hybrid perovskites. *Journal of Physical Chemistry C* **118,** 11566–11572, doi: 10.1021/jp503337a (2014).
14. D'Innocenzo, V. *et al.* Excitons versus free charges in organo-lead tri-halide perovskites. *Nature communications* **5,** 3586, doi: 10.1038/ncomms4586 (2014).
15. Yamada, Y., Nakamura, T., Endo, M., Wakamiya, A. & Kanemitsu, Y. Photoelectronic responses in solution-processed perovskite $CH_3NH_3PbI_3$ solar cells studied by photoluminescence and photoabsorption spectroscopy. *IEEE Journal of Photovoltaics* **5,** 401–405, doi: 10.1109/JPHOTOV.2014.2364115 (2015).
16. Sestu, N. *et al.* Absorption f-sum rule for the exciton binding energy in methylammonium lead halide perovskites. *J. Phys. Chem. Lett.* **6,** 4566–4572, doi: 10.1021/acs.jpclett.5b02099 (2015).
17. Soufiani, A. M. *et al.* Polaronic exciton binding energy in iodide and bromide organic-inorganic lead halide perovskites. *Appl. Phys. Lett.* **107,** 231902, doi: 10.1063/1.4936418 (2015).
18. Ishihara, T. Optical properties of PbI-based perovskite structures. *Journal of Luminescence* **60&61,** 269–274, doi: 10.1016/0022-2313(94)90145-7 (1994).
19. Valverde-Chávez, D. A. *et al.* Intrinsic femtosecond charge generation dynamics in single crystal $CH_3NH_3PbI_3$. *Energy Environ. Sci.* **8,** 3700–3707, doi: 10.1039/C5EE02503F (2015).
20. Yamada, Y., Nakamura, T., Endo, M., Wakamiya, A. & Kanemitsu, Y. Near-band-edge optical responses of solution-processed organic-inorganic hybrid perovskite $CH_3NH_3PbI_3$ on mesoporous TiO_2 electrodes. *Applied Physics Express* **7,** 032302, doi: 10.7567/APEX.7.032302 (2014).
21. Fang, H.-H. *et al.* Photophysics of organic-inorganic hybrid lead iodide perovskite single crystals. *Advanced Functional Materials* **25,** 2378–2385, doi: 10.1002/adfm.201404421 (2015).
22. Huang, L. & Lambrecht, W. R. L. Electronic band structure, phonons, and exciton binding energies of halide perovskites $CsSnCl_3$, $CsSnBr_3$, and $CsSnI_3$. *Physical Review B* **88,** 165203, doi: 10.1103/PhysRevB.88.165203 (2013).
23. Tahara, H., Endo, M., Wakamiya, A. & Kanemitsu, Y. Experimental evidence of localized shallow states in orthorhombic phase of $CH_3NH_3PbI_3$ perovskite thin films revealed by photocurrent beat spectroscopy. *J. Phys. Chem. C* **120,** 5347–5352, doi: 10.1021/acs.jpcc.6b01283 (2016).
24. De Wolf, S. *et al.* Organometallic halide perovskites: Sharp optical absorption edge and its relation to photovoltaic performance. *Journal of Physical Chemistry Letters* **5,** 1035–1039, doi: 10.1021/jz500279b (2014).
25. Yin, W.-J., Shi, T. & Yan, Y. Unusual defect physics in $CH_3NH_3PbI_3$ perovskite solar cell absorber. *Applied Physics Letters* **104,** 063903, doi: 10.1063/1.4864778 (2014).
26. Bakulin, A. A. *et al.* Real-time observation of organic cation reorientation in methylammonium lead iodide perovskites. *J. Phys. Chem. Lett.* **6,** 3663–3669, doi: 10.1021/acs.jpclett.5b01555 (2015).
27. Ma, J. & Wang, L.-W. Nanoscale charge localization induced by random orientations of organic molecules in hybrid perovskite $CH_3NH_3PbI_3$. *Nano Lett.* **15,** 248–253 (2015).
28. March, S. A. *et al.* Four-wave mixing in perovskite photovoltaic materials reveals long dephasing times and weaker many-body interactions than GaAs. arXiv:1602.05186 [cond-mat] ArXiv:1602.05186 (2016).
29. Shah, J. *Ultrafast Spectroscopy of Semiconductors and Semiconductor Nanostructures* (Springer-Verlag, 1996).
30. Segschneider, G., Dekorsy, T., Kurz, H., Hey, R. & Ploog, K. Energy resolved ultrafast relaxation dynamics close to the band edge of low-temperature grown GaAs. *Applied Physics Letters* **71,** 2779–2781, doi: 10.1063/1.120131 (1997).
31. Webber, D. *et al.* Observation of the exciton and urbach band tail in low-temperature-grown GaAs using four-wave mixing spectroscopy. *Applied Physics Letters* **105,** 182109, doi: 10.1063/1.4901180 (2014).
32. Hall, K. C., Allan, G. R., van Driel, H. M., Krivosheeva, T. & Pötz, W. Coherent response of spin-orbit split-off excitons in InP: Isolation of many-body effects through interference. *Physical Review B* **65,** 201201, doi: 10.1103/Phys-RevB.65.201201 (2002).
33. Koch, M. *et al.* Subpicosecond photon-echo spectroscopy on GaAs/AlAs short-period superlattices. *Physical Review B* **47,** 1532–1539, doi: 10.1103/PhysRevB.47.1532 (1993).
34. Gilliot, P. *et al.* Quantum beats between trion and exciton transitions in modulation-doped CdTe quantum wells. *Physical Review B* **60,** 5797–5801, doi: 10.1103/PhysRevB.60.5797 (1999).
35. Becker, P. C. *et al.* Femtosecond photon echoes from band-to-band transitions in GaAs. *Physical Review Letters* **61,** 1647–1649, doi: 10.1103/PhysRevLett.61.1647 (1988).

36. Siegner, U. *et al.* Optical dephasing in semiconductor mixed crystals. *Physical Review B* **46,** 4564–4581, doi: 10.1103/PhysRevB.46.4564 (1992).
37. Xiao, Z. *et al.* Efficient, high yield perovskite photovoltaic devices grown by interdiffusion of solution-processed precursor stacking layers. *Energy Environ. Sci.* **7,** 2619–2623, doi: 10.1039/C4EE01138D (2014).
38. Webber, D. *et al.* Measurement of coherence decay in GaMnAs using femtosecond four-wave mixing. *Journal of Visualized Experiments* **82,** e51094, doi: 10.3791/51094 (2013).

Acknowledgements
This research is supported by the Natural Sciences and Engineering Research Council of Canada.

Author Contributions
C.C. carried out the fabrication of the solution-processed $CH_3NH_3PbI_3$ film, under the guidance of I.G.H. K.C.H. conceived and designed the FWM experiments. D.W. contributed to developing the FWM apparatus. S.M. performed the FWM experiments with assistance by D.B.R. and analyzed the data. S.M. and K.C.H. wrote the manuscript with input from all authors.

Additional Information
Supplementary information accompanies this paper at http://www.nature.com/srep

Competing financial interests: The authors declare no competing financial interests.

How to cite this article: March, S. A. *et al.* Simultaneous observation of free and defect-bound excitons in $CH_3NH_3PbI_3$ using four-wave mixing spectroscopy. *Sci. Rep.* **6**, 39139; doi: 10.1038/srep39139 (2016).

Publisher's note: Springer Nature remains neutral with regard to jurisdictional claims in published maps and institutional affiliations.

This work is licensed under a Creative Commons Attribution 4.0 International License. The images or other third party material in this article are included in the article's Creative Commons license, unless indicated otherwise in the credit line; if the material is not included under the Creative Commons license, users will need to obtain permission from the license holder to reproduce the material. To view a copy of this license, visit http://creativecommons.org/licenses/by/4.0/

© The Author(s) 2016